Scientific Research Publishing

Materials Sciences and Applications, 2022, 13, 232-248
https://www.scirp.org/journal/msa
ISSN Online: 2153-1188
ISSN Print: 2153-117X

Fabrication of $ZrC/ZrB_2/C$ Composites Having High Mechanical Properties at Elevated Temperatures

Kai Matsumoto[1], Masaki Kato[1], Ken Hirota[1*], Toshiyuki Nishimura[2]

[1]Department of Molecular Chemistry & Biochemistry, Faculty of Science & Engineering, Doshisha University, Kyotanabe, Japan
[2]National Institute for Materials Science, Tsukuba, Japan
Email: *khirota@mail.doshisha.ac.jp

How to cite this paper: Matsumoto, K., Kato, M., Hirota, K. and Nishimura, T. (2022) Fabrication of $ZrC/ZrB_2/C$ Composites Having High Mechanical Properties at Elevated Temperatures. *Materials Sciences and Applications*, **13**, 232-248.
https://doi.org/10.4236/msa.2022.134013

Received: March 19, 2022
Accepted: April 26, 2022
Published: April 29, 2022

Abstract

Ultra-high temperature ceramics (UHTCs) are most recently getting much attention for structural parts of hypersonic missiles with their cruising speed of more than Mach 5. Most of the UHTCs are poor sinterability carbides, nitrides, and borides. Therefore, they have been studied and developed for a long time. However, there are still many problems to solve. In this paper, based on the solid-state reaction presented as an equation of $(x + y)\cdot ZrC + 2\cdot y\cdot B \rightarrow x\cdot ZrC + y\cdot ZrB_2 + y\cdot C$, three-phase $ZrC/ZrB_2/C$ composites have been fabricated from ZrC and amorphous B powders using pulsed electric-current pressure sintering at 1373 to 2173 K for 6.0×10^2 s under 50 MPa in a vacuum. $ZrC/ZrB_2/C$ = 30/70/C~70/30/C vol% composites with the relative densities D_r of 96.6 to 98.7% were obtained at 2073 K. The 60/40/C vol% composite revealed high bending strength σ_b (554 MPa), Vickers hardness H_v (19.2 GPa) and moderate fracture toughness K_{IC} (5.25 $MPa\cdot m^{1/2}$) at room temperature. Furthermore, all composites showed elastic deformation up to 1873 K and revealed σ_b more than 600 MPa at this temperature, in addition, some composites showed higher σ_b than 900 MPa at the same temperature. These high mechanical behaviors are discussed with those of the simple binary ZrC/ZrB_2 composites which were fabricated under the same conditions except for their starting materials. The best mechanical properties of binary composites were σ_b (474 MPa), H_v (18.5 GPa), and K_{IC} (4.45 $MPa\cdot m^{1/2}$) at room temperature, and σ_b of 400 - 700 MPa at 1873 K. Overall, three-phase composites, nevertheless including soft carbon, have higher mechanical properties than the binary composites.

Keywords

ZrC, ZrB_2, C, Composites, Pulsed Electric-Current Pressure Sintering,

Mechanical Properties

1. Introduction

Among the many kinds of engineering ceramics, ultra-high temperature ceramics (UHTCs) are materials with a high melting point T_m above 3273 K, and they have been studied and developed as structural parts working in oxidizing atmospheres at high temperatures above 2273 K [1]. Most UHTCs are carbides [2], nitrides [3], and borides [4] of early transition metals and rare earth. Strong covalent bonding between metal and C, N, and B is responsible for the high hardness, Young's modulus, and T_m. Unfortunately, monolithic UHTCs have many technical problems, such as poor oxidation resistance of carbides, the high level of difficulty in the sustainable use of mineral resources of boride HfB_2 which brings extreme high cost, and brittleness with a fracture toughness K_{IC} of 3.5 - 4.2 MPa·m$^{1/2}$ of ZrB_2 [5]. Then, an approach to producing composites has been considered to improve not only mechanical properties but also the densification and oxidation resistance of ZrB_2 ceramics [6]. An additive commonly used in the past for the production of ZrB_2-based composites was silicon carbide, SiC, with a T_m = 3003 K [7] [8] and now another covalent carbide, boron carbide (B_4C), has received much interest from material science and engineering researchers. B_4C is the third hardest material (Vickers hardness H_v = 33.5 GPa) after diamond (H_v = 75 - 100 GPa) and cubic boron nitride *c*-BN (H_v = 45 GPa). Recently, the present authors [9] fabricated B_4C/ZrB_2 composites using self-propagating high-temperature synthesis (SHS) [10] and pulsed electric-current pressure sintering (PECPS) [11] at 2173 K for 6.0 × 10^2 s under 50 MPa in a vacuum simultaneously and evaluated their mechanical properties at both room temperature R.T. and elevated temperatures up to 2023 K in an inert atmosphere. The obtained B_4C/ZrB_2 = 40/60 - 60/40 vol% composites with relative densities D_r (≥99.5%) revealed a high bending strength σ_b (≥640 MPa) from R.T. to 1873 K; the maximum value of 803.5 MPa was observed for the 60 vol% B_4C composite at 1873 K.

To improve the high-temperature σ_b much more, other additives have been studied based on the idea that the additive should be a Zr compound, which should have a higher T_m than B_4C (T_m: 2724 K), along with the role of sintering aids. Then, ZrC was selected because its T_m is 3533 K. However, the mixed powder compacts consisting of high-temperature refractory substances were considered to show poor sinterability. Furthermore, only a few reports described the fabrication of simple binary-system ZrC/ZrB_2 composites. In 2007, Tsuchida *et al*. [12] reported a series of ZrC/ZrB_2 composites concerning the powder preparation using mechanical activation-assisted SHS (MA-SHS), and the materials sintered by spark plasma sintering (SPS) [13], *i.e*., PECPS, at 2073 K for 3.0 - 6.0 × 10^2 s under 40 MPa in a vacuum. They evaluated the mechanical

properties of ZrC/ZrB_2 composites at R.T., which were started from the mixtures of Zr/B/C = 4/2/3 to 6/10/1 molar ratio elemental powders; *i.e.*, they were presented as chemical compound ratios, such as (ZrC/ZrB_2 = 3/1 - 1/5 molar ratios). Those authors reported that the highest H_v of 17.8 GPa and K_{IC} of 4.8 $MPa{\cdot}m^{1/2}$ were attained at ZrC/ZrB_2 = 1/1 and 1/2 molar ratios, respectively. On the other hand, Neuman *et al.* [14] produced dense bullets of 9.5 vol%ZrC - 0.1 vol%C - 90.4 vol%ZrB_2 by hot-pressing at 2173 K and reported their σ_b and K_{IC} at ambient temperature to 2573 K; σ_b and K_{IC} were (695 MPa, 4.8 $MPa{\cdot}m^{1/2}$) at ambient temperature, (300 MPa, 3.4 - 4.5 $MPa{\cdot}m^{1/2}$) at 1673 - 1873 K, and (345 MPa, 3.6 $MPa{\cdot}m^{1/2}$) at 2073 - 2173 K.

In the present study, we tried to prepare dense ZrC/ZrB_2-based composites from the mixed powders of ZrC and amorphous B by utilizing PECPS. Thus, fabricated three-phase $ZrC/ZrB_2/C$ composites revealed high σ_b more than 600 MPa at 1873 K. In addition, some composites showed higher σ_b than 900 MPa at the same temperature. The present paper describes the relationship between their mechanical properties and compositions in comparison with those of simple binary ZrC/ZrB_2 composites sintered under the same conditions except for the starting materials of Zr, B, and ZrC.

2. Experimental Procedure

2.1. Preparation of Composites

The fabrication procedure of $ZrC/ZrB_2/C$ composites is as follows. The starting powders were ZrC (Japan New Metals, Osaka, Japan; average particle size P_s of ϕ2.0 μm, purity of 98.5%, theoretical density D_x of 6.634 $Mg{\cdot}m^{-3}$ (Powder Diffraction File, PDF: #35-0784) and amorphous B (H.C. Starck, Goslar, Germany; grade I, P_s of ϕ0.2 μm, purity ≥ 95%, D_x of 1.73 $Mg{\cdot}m^{-3}$ [15]). ZrC and amorphous B powders were weighted into the desired ratios to fabricate $ZrC/ZrB_2/C$ composites with the compositions of (24.97 - 64.44) vol% ZrC/(58.27 - 27.62) vol% ZrB_2/(16.76 - 7.94) vol% C; in other words, the main components of ZrC/ZrB_2 = 30/70~70/30 vol%, as shown in Table 1. They were synthesized by solid state reaction presented by the following Equation (1):

$$(x+y)\cdot \mathrm{ZrC} + 2y\cdot \mathrm{B} \rightarrow x\cdot \mathrm{ZrC} + y\cdot \mathrm{ZrB_2} + y\cdot \mathrm{C} \quad (1)$$

Here, it should be noted that the compositions in Table 1 are displayed in vol% because when we discuss the mechanical properties of composites, their components should be presented in vol%. Therefore, "mol" in Equation (1) is transformed into "vol" in Table 1. For example, in order to fabricate ZrC/ZrB_2 = 50/50 vol% composite, x = 3.214 and y = 2.706 are calculated based on the values of dD_x(ZrC) = 6.634, $D_x(ZrB_2)$ = 6.104 (PDF: #34-0423), and D_x(C) = 2.26 $Mg{\cdot}m^{-3}$ (PDF: #19-178)] and their molecular weights.

The ZrC and B mixed powders were dispersed into ethanol by an ultrasonic vibrating homogenizer with a 300 W output power at a frequency of 20 kHz (US-300T, Nihon Seiki, Tokyo, Japan) for 1.80×10^3 s. The obtained slurries

Table 1. Bulk, theoretical, and relative densities of ZrC/ZrB_2/C composites.

Composition			Bulk density	Theoretical density[+]	Relative density
ZrC (vol%)	ZrB_2 (vol%)	C (vol%)	D_{obs} (Mg·m^{-3})	D_x (Mg·m^{-3})	D_r (%)
30* (24.97)[#]	70* (58.27)[#]	-* (16.76)[#]	5.40	5.592	96.6
40* (34.11)[#]	60* (51.17)[#]	-* (14.72)[#]	5.60	5.719	97.9
50* (43.71)[#]	50* (43.71)[#]	-* (12.57)[#]	5.75	5.853	98.2
60* (53.81)[#]	40* (35.87)[#]	-* (10.32)[#]	5.96	6.041	98.7
70* (64.44)[#]	30* (27.62)[#]	-* (7.94)[#]	6.03	6.140	98.2

[+]: calculated using D_x(ZrC) = 6.634 Mg·m^{-3} (PDF:#35-784), D_x(ZrB_2) = 6.104 Mg·m^{-3} (PDF:#34-423) and D_x(C) = 2.26 Mg·m^{-3}. *: vol% presented as ZrC/ZrB_2 ratio. [#]: vol% presented as ZrC/ZrB_2/C ratio.

were dried at room temperature in air, after a small amount of Acrylic/PVA 3 mass % solution was added as a binder to the dried dispersed powders, and mixed using an alumina mortar and pestle for 1.80×10^3 s. The mixtures were uniaxially compacted into a disk with a 20 mm diameter and a ~7 mm thickness at 75 MPa, and then cold isostatically pressed (CIP) at 245 MPa for 1.80×10^2 s.

The CIPed dense green compact, corresponding to ZrC/ZrB_2 = 50/50 vol%, with a bulk green density D_{bulk}(g) of 3.15 - 3.16 Mg·m^{-3} estimated from the volume and weight, was wrapped with a hexagonal BN powder (P_s: f3 μm) and put into a cylinder mold (inner diameter ϕ22 mm, outer diameter ϕ42 mm, height 30 mm) with two cylindrical plungers (diameter ϕ21.5 mm and height 30 mm) made of high-density graphite. The powder compacts were densified by PECPS (SPS-5104A, SPS SYNTEX, Yokohama, Japan) at various temperatures (1273 - 2173 K) under a uniaxial pressure of 50 MPa for 6.0×10^2 s in a vacuum (~50 Pa) with a heating rate of 1.666 K·s^{-1}d applying DC pulsed electric current (on/off interval = 12:2). Above 873 K, the heating temperature was monitored at the center position of the outside wall of the carbon mold by a monochrome pyrometer. Since this powder compact sintered at 2073 K archived the highest relative density D_r of 98.2% (details of this result will be discussed later), the powder compacts with the various ZrC/ZrB_2 compositions (*i.e.*, 30/70-70/30 vol%, **Table 1**) were sintered at 2073 K/50MPa/6×10^2s/vacuum under the same conditions described above.

Furthermore, to investigate the effects of carbon included in the composites on their mechanical properties, simple binary ZrC/ZrB_2 composites without C were also fabricated using PECPS of the mixed powders of Zr, B, and ZrC. Their powder characteristics were as follows: Zr (Kojundo Chemical Laboratory, Saitama, Japan; P_s of ϕ10 μm, purity of 98%, D_x of 6.505 Mg·m^{-3} (PDF: #5-0665) delivered in immersed, fine amorphous B (H.C. Starck; grade I, P_s of ϕ0.03 μm, purity ≥ 95%, D_x of 1.73 Mg·m^{-3}) and the same ZrC powder as mentioned above. Here, a very fine amorphous active B powder was adopted so as to react with large Zr powder. The desired mixed powders, aiming at final compositions with

ZrC/ZrB_2 = 40/60, 50/50, 60/40, 70/30 vol%, were compacted and sintered under the same conditions as the $ZrC/ZrB_2/C$ composites.

2.2. Characterization

Phase identification of powders and composites was made by X-ray diffraction (XRD; Smartlab, Rigaku, Tokyo, Japan) analysis using Cu*Ka* radiation (a wavelength of 0.15418 nm). The bulk density D_{bulk} of dense materials was measured by Archimedes' method, and relative density D_r was estimated based on theoretical density D_x ($Mg{\cdot}m^{-3}$) which was calculated using the values of 6.634 for ZrC, 6.104 for ZrB_2, and 2.26 for C. Microstructural observation using a field-emission-type scanning electron microscope (FE-SEM; SU8020, Hitachi High-Technologies, Tokyo, Japan) equipped with an energy-dispersive X-ray spectroscope (EDS, JED-2300/F, JEOL, Tokyo, Japan) was performed. After phase identification, test bars for mechanical-property measurements were cut from the sintered materials with a diamond cutting blade and then their upper and lower surfaces were polished to mirror surfaces with a diamond paste (nominal P_s: ϕ1 - 3 μm); the other two sides were grinded with a diamond abrasive tool containing #400 grid-pass diamond particles.

2.3. Evaluation of Mechanical Properties

At room temperature, various mechanical properties of composites were measured: three-point bending strength σ_b was evaluated with a crosshead speed of 8.33×10^{-6} $m{\cdot}s^{-1}$ and an 8.0 mm span length using WC jigs. Vickers hardness H_v and fracture toughness K_{IC} were estimated with an applied load of 196 N for 15 s for the former and the indentation fracture method (IF) with Niihara's equation [16] for the latter.

On the other hand, high-temperature bending strength σ_b of $ZrC/ZrB_2/C$ composites was measured from 1273 to 2023 K in Ar using an AG-X Plus autograph (Shimadzu, Kyoto, Japan) at the National Institute for Materials (NIMS), Tsukuba, Ibaraki, Japan. Samples were heated at a rate of 0.5 $K{\cdot}s^{-1}$ by tungsten heater elements. After the predetermined temperature was reached, three-point bending tests were carried out (a span length of 10.0 mm, a crosshead speed of 8.33×10^{-6} $m{\cdot}s^{-1}$) by using a B_4C jig. During this test, a set of load displacements was measured to evaluate the stress-strain (σ - ε) curves as a function of testing temperature.

3. Results and Discussion

3.1. Simultaneous Synthesis and Densification of $ZrC/ZrB_2/C$ Composites

Hereafter, we sometimes denote the composite as the final composition, e.g., $ZrC/ZrB_2/C$ = 43.71/43.71/12.5 7vol% = 50/50/C vol%, "50Zr-C", here, we add "-C" in order to distinguish between three-phase $ZrC/ZrB_2/C$ and binary-phase ZrC/ZrB_2 composites. As described in 2. Experimental procedure, a CIP-ed

sample corresponding to 50ZrC-C was utilized to investigate the effects of PECPS temperature on the formation and densification of materials. The bulk density of the cylindrical green powder compacts [D_{bulk}(g)] was about 3.15 - 3.16 Mg·m^{-3}, and its relative density [D_r(g)] was estimated to be 67.6% - 67.7%; these values were calculated using the theoretical density [D_x(g)] of 4.656 Mg·m^{-3} obtained from the D_x values of 6.634 Mg·m^{-3} of ZrC and 1.73 Mg·m^{-3} of B.

In order to investigate the crystalline phase change during PECPS, the ZrC/B mixed powder compacts were sintered at various temperatures from 1273 K to 2173 K for 6.0×10^2 s in a vacuum (~50 Pa) and many corresponding test pieces were prepared. XRD patterns of sintered samples with Si powder as an internal standard which had been added to determine their lattice parameters precisely are shown in Figure 1, in addition to that of the starting mixture. At a glance, it is difficult to recognize the formation of ZrB_2 at 1273 K. However, in the XRD patterns measured at 1373 K, a small diffraction peak of the ZrB_2 phase is observed around $2\theta = 42^\circ$ and there are only two phases: ZrC (PDF: #35-0784) and ZrB_2 (PDF: #34-0423) up to 2173 K; graphite C and B_4C phases are not recognized, which might be due to a much smaller diffraction peak compared with those of Zr-based compounds. The formation of graphite C is confirmed by the SEM-EDX observation, which will be described later.

A precise Rietveld analysis was performed on these XRD patterns; the crystallite sizes (X_s) of ZrC and ZrB_2, and the lattice parameters a of cubic ZrC, a and c of hexagonal ZrB_2 phases in the materials obtained at room temperature to 2173 K were investigated. Table 2 shows their results: as far as X_s is concerned, the particle size P_s of ZrC of starting material was around ϕ2.0 μm, however, its X_s was around f100 nm, indicating starting ZrC was a polycrystal powder. Each ZrC particle was attacked by amorphous active B particles around 1273 K, then the contact area on the surface of ZrC changed into a very small ZrB_2 (X_s ~f2.0

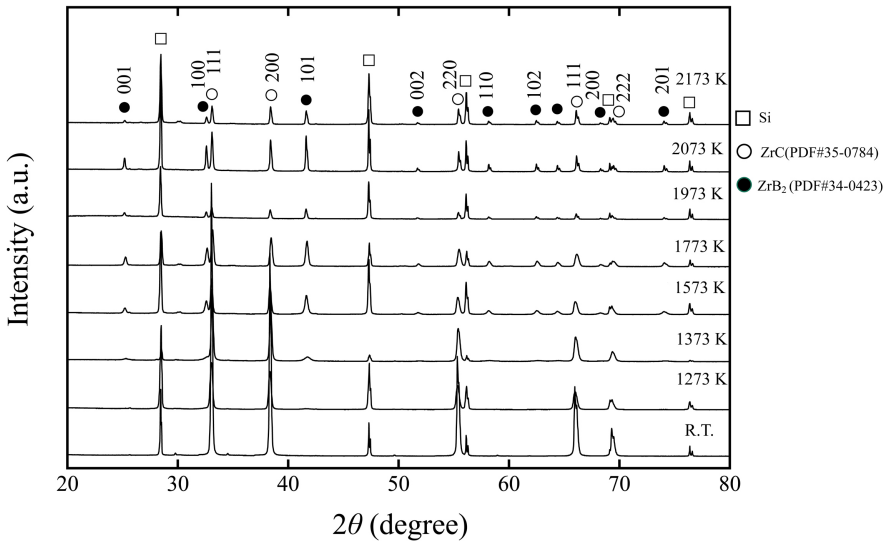

Figure 1. XRD patterns of mixed powder (ZrC/B) samples heated at various temperatures using PECPS, corresponding to ZrC/ZrB_2/C = 50/50/C vol%.

Table 2. Crystalline phase information about the products obtained at various PECPS temperatures.

Crystalline phases & crystallite size (nm)			Lattice parameter of ZrC	Lattice parameters of ZrB_2	
Sample	ZrC	ZrB_2	*a* (nm)	*a* (nm)	*c* (nm)
mixture	100.0 (121)		0.46896		
1000˚C	37.3 (16)	1.9 (6)	0.46945	0.3137	0.3523
1100˚C	66.1 (139)	14.5 (12)	0.46946	0.3170	0.3510
1300˚C	64.7 (127)	29.6 (11)	0.46919	0.3170	0.35319
1500˚C	48.4 (49)	34.1 (5)	0.46865	0.3170	0.35313
1700˚C	55.6 (20)	44.2 (15)	0.46919	0.3174	0.35425
1800˚C	58.1 (10)	55.4 (14)	0.46882	0.3173	0.35337
1900˚C	55.7 (7)	46.9 (14)	0.46844	0.3170	0.35331

*Si was used as an external standard. ZrC (PDF#35-0784), cubic: a = 0.46930 nm, ZrB_2 (PDF: #34-423), hexagonal: a = 0.316870, c = 0.353002 nm.

nm) + C. The X_s of ZrB_2 grew gradually from f2.0 nm at 1273 K to f47 nm at 2173 K. On the other hand, the X_s of ZrC decreased gradually from ϕ100 nm (R.T.) to f56 nm (2173 K), as it had been eroded by active B. As the lattice parameters of both ZrC and ZrB_2 were almost constant and agreed with the reported PDF data, they did not form a solid solution during active PECPS, as reported in an equilibrium phase diagram of ZrC-ZrB_2 [17].

The microstructures of the composites fabricated at various temperatures were observed and their bulk densities were measured. **Figure 2** shows SEM photographs of the samples sintered at 1373 K to 2173 K for $6.0 \cdot 10^2$ s. Their D_r values are also inserted into the SEM photographs. Between 1373 K and 1773 K, the microstructures changed little: mainly large f2.0 μm ZrC and fine f0.2 μm B particles are recognized with nearly the same D_r of 62%. This value is smaller than that (67.6% - 67.7%) of the starting powder compact. The difference must be due to the crystalline phase change from (ZrC/B) to (ZrC/ZrB_2/C), followed by the changes in D_x (4.656 $Mg \cdot m^{-3}$) and D_x (5.853 $Mg \cdot m^{-3}$) for the former and the latter, respectively. However, from 1973 K the sample begins to be densified into 77.2%. At 2023 K, the SEM photograph of the composite indicates a change in microstructural morphology: relatively finer grains agglomerated with each other instead of remaining isolated particles, suggesting the dynamic reconstructive reaction of (ZrC + 2·B → ZrB_2 + C) and resulting in the formation of ZrB_2 accompanied by much higher densification around 87%. When the composite was heated to 2073 K, sintering reached the final stage with a D_r of 98.2%, and grain growth to several microns was observed. Upon further heating to 2173 K, the D_r value was the same, suggesting almost the completion of densification at 2073 K, and the grain sizes (G_s) of ZrC and ZrB_2 were also unchanged. Here, the volume change from the mixture of ZrC and B to the composite of ZrC/ZrB_2/C

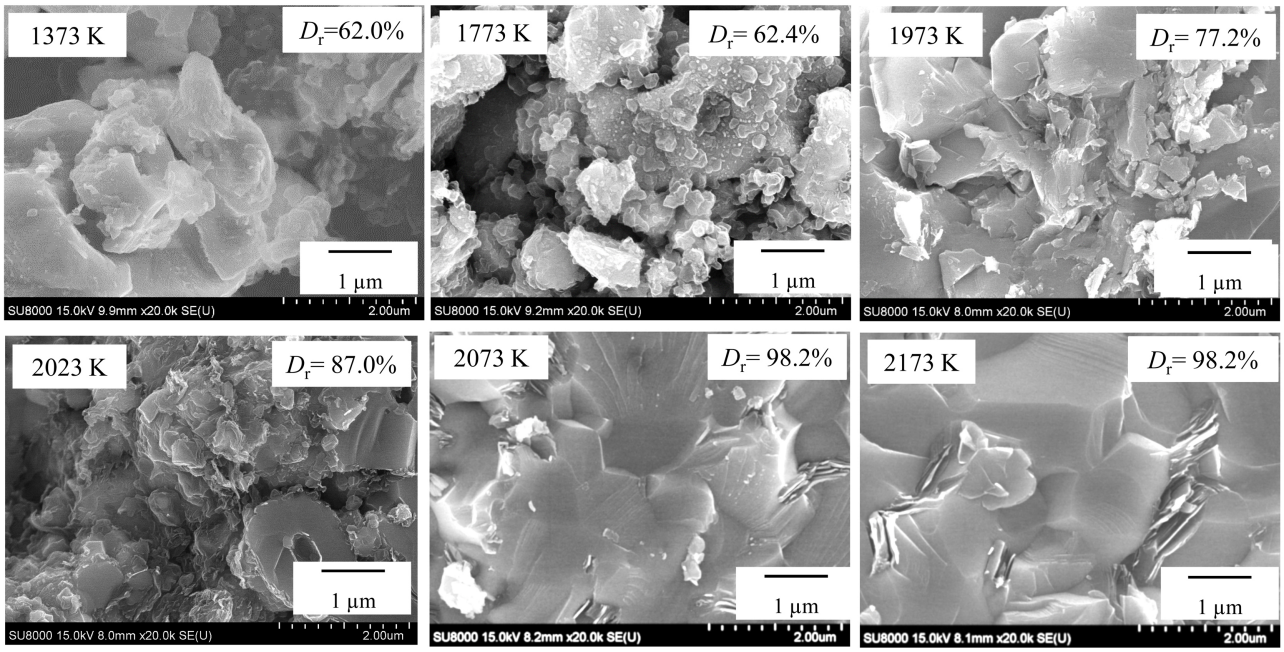

Figure 2. SEM photographs of the fractured surfaces of ZrC/ZrB_2/C = 50(43.71)/50(43.71)/(12.57) vol% composites fabricated at various temperatures using pulsed electric-current pressure sintering (PECPS).

was considered. In the case of the composition of ZrC/ZrB_2/C = 50/50/C vol%, a volume change ratio D*V*/V_o, here, D*V* is a volume change after phase change, V_o is a starting volume, is about - 2.02%, which is calculated from the values of D_x(ZrC) = 6.634, D_x(amorphous B) = 1.73, D_x(ZrB_2) = 6.104, and D_x(C) = 1.26 $Mg{\cdot}m^{-3}$. This D*V*/V_o = −2.02% means that it is difficult to crush up or densify the ZrC/ZrB_2/C composite up to the theoretical density by an ordinal uniaxial pressure of 50 MPa during PECPS. Hereafter, based on these results, all composites were sintered at 2073 K. The microstructures of ZrC/ZrB_2/C composites fabricated at 2073 K were then observed. **Figure 3** upper stand shows SEM photographs of their fractured surfaces, and D_r values are also presented. The D_r reaches the top value of 98.7% around the 60ZrC-C composite, *i.e.*, ZrC/ZrB_2/C = 60(53.81)/40(35.87)/(10.32) vol% as shown in **Table 1**.

Here we have to mention the fabrication of simple binary ZrC/ZrB_2 as abbreviated as 40ZrC to 70ZrC composites. The XRD patterns of materials sintered at 2073K showed that the composites consisted of only two components of ZrC and ZrB_2, indicating that the solid-state reaction between Zr and B was completed at 2073 K. The 40ZrC-70ZrC composites showed D_r values higher than 99.9%; their SEM photographs are displayed in **Figure 4**. Both 50ZrC and 60ZrC composites show full densified microstructures with well-developed grains. If we compare the 99.9% value with the D_r of ZrC/ZrB_2/C composites, this difference might be explained in terms of the lower melting point T_m of Zr than ZrC: *i.e.*, T_m (Zr) = 2128 K is 1405 K lower than T_m (ZrC) = 3533 K, nevertheless, there is much higher volume reduction, *DV*/V_o, *i.e.*, the *DV*/V_o values are estimated to be from −20.66% (40 vol%ZrC) to −11.52% (70 vol%ZrC). Therefore, these high

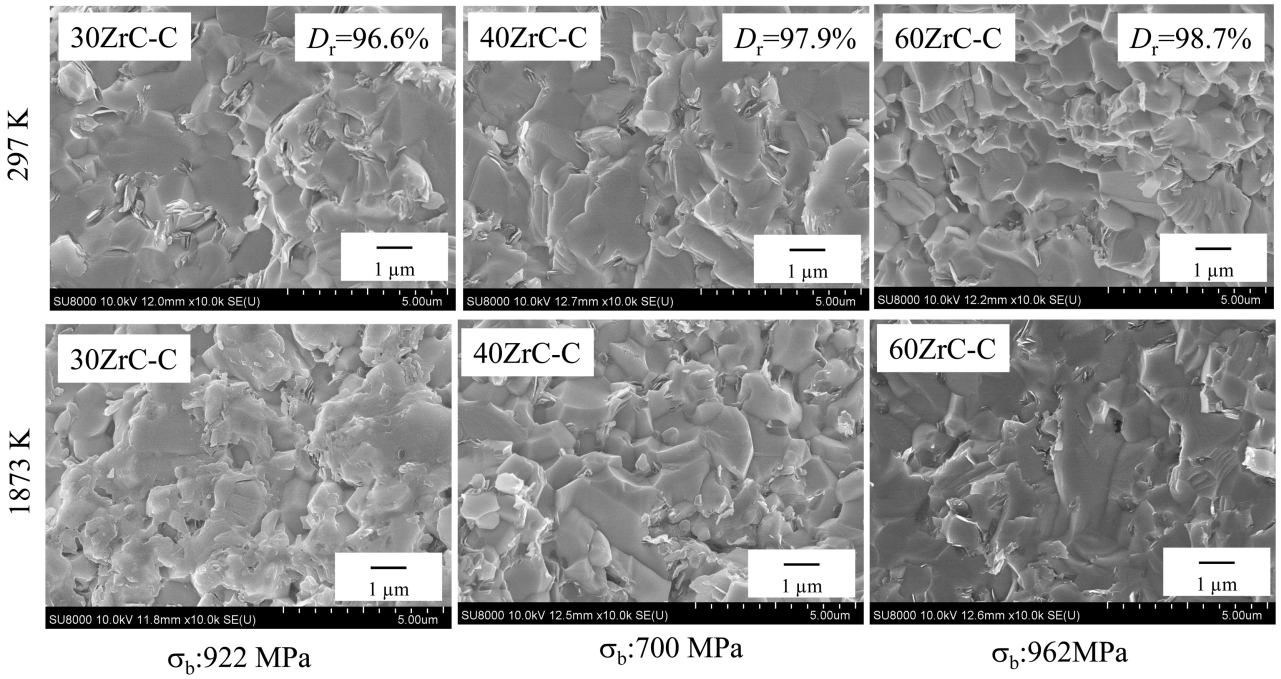

Figure 3. SEM photographs for the fracture surfaces of ZrC/ZrB_2/C = 30/70/C, 40/60/C and 60/40/C vol% composites at 297 K and 1873 K in Ar.

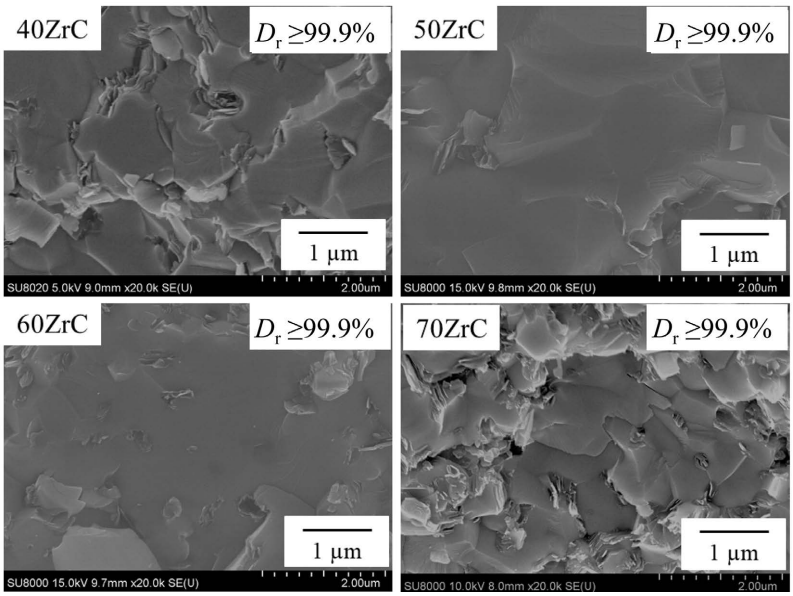

Figure 4. SEM photographs for the fracture surfaces of ZrC/ZrB_2 composites fabricated at 2073 K. Here, "40ZrC" means ZrC/ZrB_2 = 40/60 vol% composite.

densities might be achieved by plastic deformation of soft Zr at only 55 K lower temperature than T_m (Zr) = 2128 K during PECPS.

3.2. Mechanical Properties of Two-Phase and Three-Phase Composite at R.T. and High-Temperatures

Then, the mechanical properties of ZrC/ZrB_2/C composites, such as three-point

bending strength σ_b, Vickers hardness H_v, and fracture toughness K_{IC}, were measured at room temperature. Figure 5 displays these properties as a function of ZrC volume content *vs.* ZrB_2. The σ_b increases from 460 (30ZrC-C) to 555 MPa (60ZrC-C) and decreases gradually to 510 MPa (70 volZrC-C). The H_v values start from 13.2 to 19.2 GPa around 60ZrC-C and then pitch downward to 13.4 GPa. The K_{IC} takes also a constant value of 5.0 ± 0.25 MPa·m$^{1/2}$. It should be noted that all the highest values of σ_b and H_v are attained at 60ZrC-C composite. In general, the strength of inorganic composites depends much on their composition, relative density, grain and pore sizes, and distribution, and even on the preparation process. On the other hand, the hardness H_v of a composite obeys the mixing rule that H_v (composite) is the summation of H_v from each component. As each component's H_v values of ZrC and ZrB_2 are 25.48 and 21.56 GPa, respectively [18], H_v of ZrC/ZrB_2/C composite could increase with increasing ZrC content. However, in the present composites, H_v (70 vol% ZrC-C) decreases rapidly from 19.2 to 13.4 GPa. This might be explained in terms of 1) grain growth from f2~3 μm to f3~4 μm and 2) a small decrease in relative density from 98.7% (60ZrC-C) to 98.2% (70ZrC-C) and; these factors are strongly related to the reduction in the H_v value. The K_{IC} depends on the microstructure, especially grain size G_s of composites having the same composition and density. These factors might explain why the 60ZrC-C composite has the highest K_{IC} value among ZrC-C composites. Furthermore, in order to study the effect of graphite addition, the mechanical properties of binary ZrC/ZrB_2 composites were measured as a counterpart. Table 3 1) and 2) present their properties at room and high temperatures, respectively. As a whole, σ_b, H_v, and K_{IC} at R.T., *i.e.*, the highest values of σ_b (474 MPa), H_v (18.5 GPa), and K_{IC} (4.45 MPa·m$^{1/2}$),

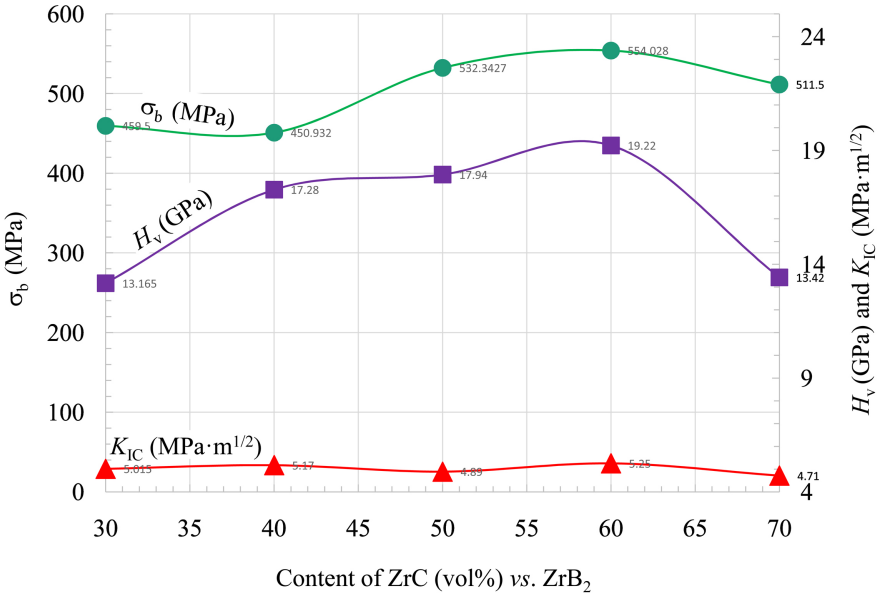

Figure 5. Mechanical properties, bending strength σ_b, Vickers hardness H_v and fracture toughness K_{IC} of ZrC/ZrB_2/C composites at room temperature as a function of ZrC content (vol%) *vs.* ZrB_2.

Table 3. Mechanical properties of ZrC/ZrB_2 composites at (a) room temperature and (b) high-temperatures.

(a)

Composition	at 293 K		
ZrC (vol%)	σ_b	H_v (GPa)	K_{IC} (MPa·$m^{1/2}$)
40	420	18.1	4.09
50	474	18.5	4.11
60	355	17.8	4.45
70	347	14.7	3.96

(b)

Composition	Three-point bending strength σ_b (MPa) at				
ZrC (vol%)	1273 K	1473 K	1673 K	1873 K	2023 K
40	383	401	561	701	435
50	485	443	423	520	407
60	445	466	561	416	534
70	550	526	595	272	622

are not so high as compared with those for ZrC-C composites in **Figure 5**. Based on common sense about the mechanical properties of composites, as graphite has low σ_b, H_v, and K_{IC}, three-phase composites should have lower mechanical properties. However, the experimental results show the opposite. This could be explained by the differences in preparation routes, as follows:

1) As the binary composites (ZrC/ZrB_2) were prepared from the mixture of (Zr, B, ZrC), the binding force between ZrB_2 and ZrC grains might be weak, because a strong solid-state reaction could be introduced only between Zr and B, forming ZrB_2 grains.

2) On the contrary, in the three-phase composites (ZrC/ZrB_2/C), the binding force between ZrB_2 and ZrC through their interface/grain boundary should be strong because ZrB_2 grains were formed from ZrC by attacking B particles and separated from ZrC during PECPS. Nevertheless, there exist soft C grains among them.

Next, we address the main purpose of the present study: to evaluate high-temperature σ_b and toughness. **Figure 6** shows σ_b of all ZrC-C composites as a function of measurement temperatures from 1273 to 2023 K. The σ_b values previously reported on the simple ZrC/ZrB_2 = 10/90 vol% composite [14] are also plotted as a reference. Overall, it is clear that the σ_b values at 1273 K of all ZrC-C composites are higher than those at ambient temperature, and at 1873 K some composites reveal the highest σ_b values in a series of compositions, *i.e.*, the 30 and 60ZrC-C composites showed σ_b of 922 and 962 MPa, respectively. These values are much higher than that (301 MPa) reported previously [13], and our previous high-temperature σ_b value (803.5 MPa) attained for B_4C/ZrB_2 = 60/40 vol%

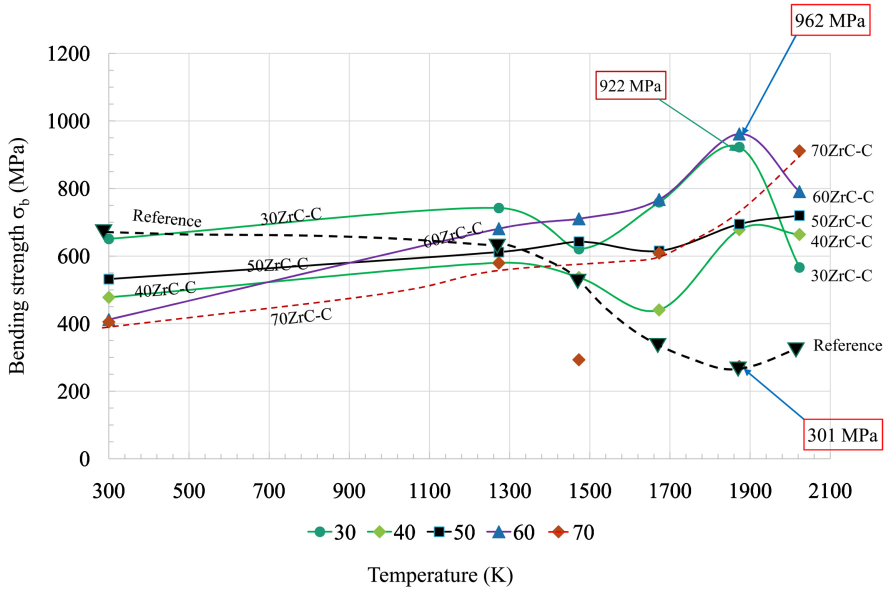

Figure 6. Bending strength σ_b of $ZrC/ZrB_2/C$ composites at various temperatures in Ar.

composites [9].

Among many ultra-high temperature ceramics (UHTC), such as boride, carbides, and nitrides, there is little information on three-point σ_b above 900 MPa at 1873 K. In addition, only a few reports [12] [14] describe the fabrication processes and mechanical properties of simple ZrC/ZB_2 composites at both room and elevated temperatures. However, no detailed study has been published up to now.

Many points of view have been taken to explain why 60ZrC-C composite shows such high s_b. After much consideration, it might be explained mainly in three ways. First, the high content of ZrC (60 vol% *vs.* ZrB_2), of which T_m (3533 K) [18] and Young's modulus E (500 GPa) [18] are 220 K and 152 GPa higher than those (T_m: 3313 K, E: 348 GPa) of ZrB_2 [18], respectively; these two factors have much influence on strength. Second, the binding force between ZrC and ZrB_2 grains must be strong, as mentioned before. In addition, the dislocation could form at the interface between cubic ZrC and hexagonal ZrB_2 grains. Of course, the latter originates from the ZrC-B contact area. This dislocation, especially edge dislocation, might play an important role in high-temperature strength. Third, the 60ZrC-C composite consists of smaller grains, in addition to relatively high D_r (98.7%), as shown in **Figure 7**.

On the other hand, it is difficult to explain why the 30ZrC-C composite revealed a high σ_b (922 MPa) at 1873 K. One reason might be a large amount of graphite (as shown in **Table 1**) at the grain boundary between carbide and boride. This graphite can connect the grains of ZrC and ZrB_2 strongly, with the inverse temperature dependence of the strength of graphite C: the higher the temperature, the higher the strength. Another reason is their smaller G_s, irrespective of the lower D_r. Therefore, the best composition for the three-phase composites could be determined by the balance among the interface area of ZrC/ZrB_2, the

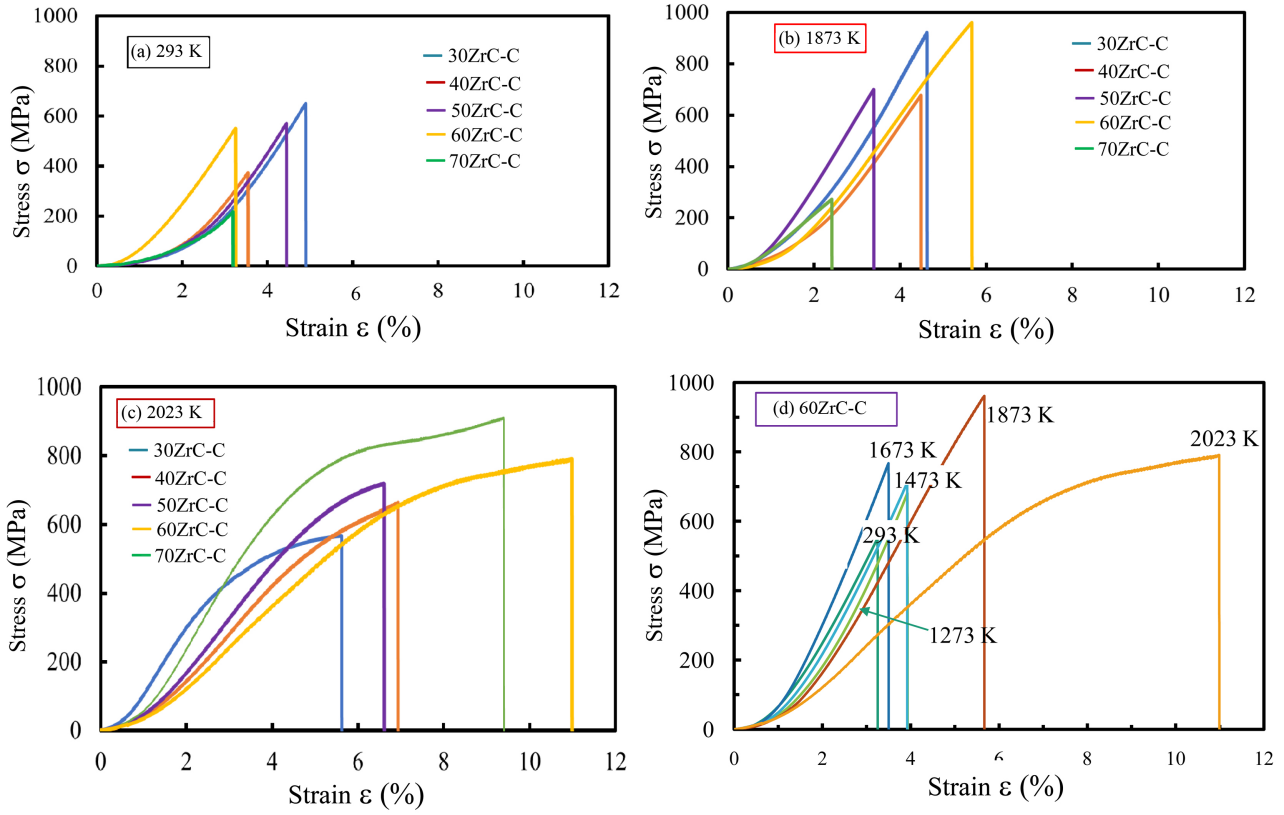

Figure 7. Stress-strain (σ - ε) curves of all composites measured at (a) 293 K, (b) 1873 K, and (c) 2023 K. And (d) σ - ε curves of 60ZrC-C at various temperatures.

content of ZrC, and the amount of graphite C and its distribution.

Here, we evaluated the high-temperature σ_b of binary ZrC/ZrB_2 composites and compared them with those of three-phase ZrC/ZrB_2/C composites. The σ_b values, as shown in **Table 3(b)**, are lower than expected. Of course, these simple composites revealed elastic deformation up to 1873 K and plastic deformation at 2023 K, the same as ZrC/ZrB_2/C composites, the latter of which will be described. These phenomena could support the additional effect of graphite superficially. At first, it was considered that if graphite is contained in the composites, their mechanical properties will be reduced by soft graphite. However, when we compared these mechanical properties at room and high temperatures, we found that graphite addition can bring good mechanical properties.

For a two-phase composite, the best composition is 40ZrC. This suggests that the mechanical properties might much depend on the ZrB_2 content; because 1) the difference in the thermal expansion coefficient a between ZrC (7.06×10^{-6} K^{-1}) [18] and ZrB_2 (6.98×10^{-6} K^{-1}) [18] is small; and 2) the binding force between base ZrB_2 grains could control the mechanical properties of composites, then the 40ZrC (60 vol% ZrB_2) composite revealed high σ_b at elevated temperatures. However, the reason why the σ_b values of both two- and three-phase composites tend to drop at 2023 K except for 70ZrC-C composite still remained.

At this stage, we paid much attention to the fracture modes, *i.e.*, elastic and

plastic deformations. The stress-strain (σ - ε) curves of all composites were measured at various temperatures. Figure 7 displays representative σ - ε curves measured at (a) 293, (b) 1873, and (c) 2023 K. In (a) and (b), all σ - ε curves exhibit elastic deformation. However, in (c) composites fractured after plastic deformation. From a practical viewpoint, applicable composites must be used in the elastic deformation field. Then it should be noted that the top σ_b values are attained within the elastic deformation field. Figure 7(d) focuses on the 60ZrC-C composite, which has the highest σ_b, its σ - ε curves are summarized as a parameter of measurement temperatures. It is clear that the fracture mode changes from elastic to plastic deformation between 1873 K and 2023 K. The microstructural changes in the elastically fractured surfaces of the composites of 30ZrC-C, 40ZrC-C, and 60vZrC-C at room temperature (297 K) and at high temperature (1873 K) were compared. As mentioned before, the upper and lower three SEM images in Figure 3 are the rupture cross-sections of these ZrC-C composites fractured at 297 K and 1873 K, respectively. We find little change in grain size, pore distribution, or dense texture. Furthermore, at the same temperature, *i.e.*, along with the horizontal line, there is no drastic change in microstructure among them.

3.3. The Microstructural Change of Composites at High Temperatures

Next, by focusing on the 60ZrC-C composite, the microstructural change between elastically fractured at 1873 K and plastically fractured at 2023 K was precisely compared using SEM+EDS elemental mapping. Here we have to mention what we call "carbon contamination in SEM", which is sometimes caused by the oil-vacuum pump system. However, as the present SEM + EDS system adopted a rotary + turbo molecular pump system, the vacuum space chamber is almost free from carbon contamination. This new concept is widely known and common knowledge to many researchers who treat this advanced SEM equipped with a "rotary + turbo molecular pump system" as a vacuum pump. The upper images in Figure 8 show various SEM photographs of 1873 K- fractured surfaces, such as secondary electron image SEM with an elemental concentration distribution, SEM + Zr, SEM + C, and SEM + B. The lower images show 2023 K-fractured surfaces. Although ZrC and ZrB_2 grains are discriminated by dense-colored areas, which indicate high concentrations of corresponding elements, it is very difficult to find the graphite C among the matrix. In Figure 8, by pointing to C, ZrC, and ZrB_2 grains, we tried to distinguish microstructures between 1873 K- and 2023 K-fractured surfaces, but there was little difference. Therefore, we might speculate that plastic deformation, followed by fracture, occurred along the hexagonal (001) slip plane of graphite or edge dislocation. And generally speaking, based on a sintering temperature of 2073 K, sintered materials might begin to deform plastically around 50 - 100 K below the sintering temperature, *i.e.*, 2023 K - 1973 K. This phenomenon introduced by plastic deformation under 50 - 100 K below the sintering temperature is often used for densifying

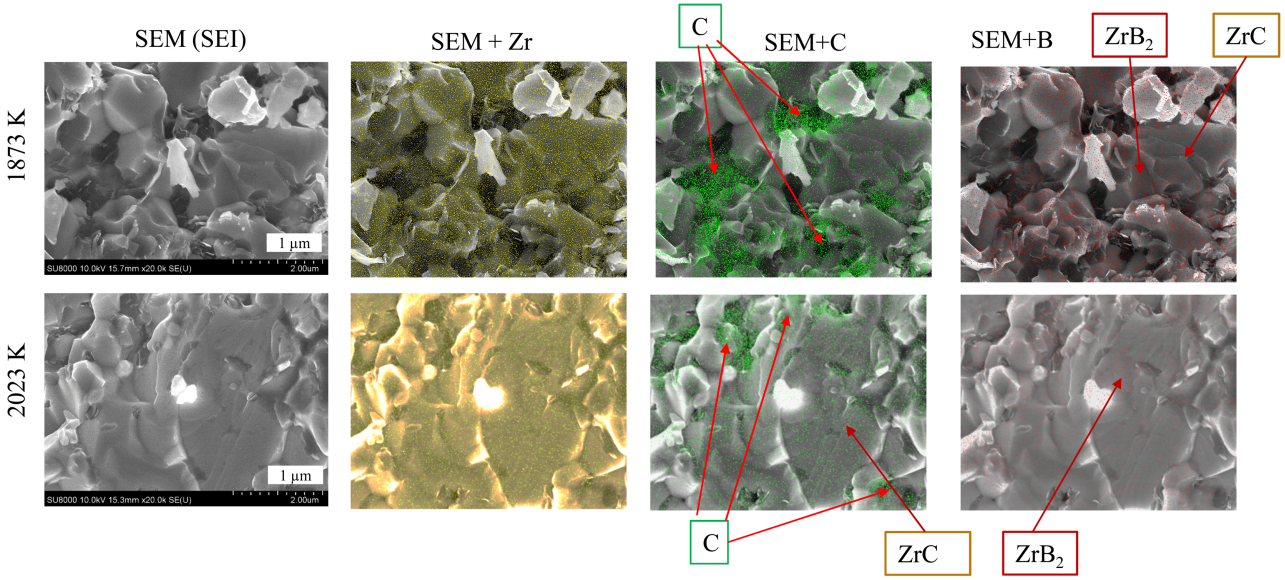

Figure 8. Various SEM photographs for the fracture surfaces of 60ZrC-C composites at 1873 K and 2023 K in Ar.

poorly sinterable inorganic material by hot isostatic pressing (HIP). This is based on an empirical rule: at these temperatures, inorganic material will deform plastically into dense materials. If the present rule is also applicable to ZrC/ZrB_2-based composites, the plastic deformation of all composites could be explained.

4. Conclusions

Based on a new idea, three-phase UHTC ZrC/ZrB_2/C composites consisting of carbides and boride were simultaneously synthesized and sintered. Dense (25 - 64) vol% ZrC/(58 - 28) vol% ZrB_2/(17 - 8) vol% C composites with D_r of 96.6% - 98.7% were fabricated by pulsed electric-current pressure sintering (PECPS) at 2073 K for 6.0×10^2 s under 50 MPa in a vacuum from the mixed powders of ZrC and amorphous B. Samples containing 60 vol% ZrC *vs.* ZrB_2, *i.e.*, 60Zr-C composite exhibited the optimized mechanical properties at R.T.: σ_b of 555 MPa, H_v of 19.2 GPa, and K_{IC} of 5.0 MPa·$m^{1/2}$. Furthermore, this composite showed the highest σ_b value of 962 MPa even at 1823 K. In comparison with σ_b of binary-phase ZrC/ZrB_2 composites, this extreme high σ_b was attributed to the following factors: 1) the high content of ZrC (60 vol% *vs.* ZrB_2), 2) the strong binding force between ZrC and ZrB_2 grains, 3) the relatively high D_r (98.7%), and 4) the smaller grain size.

This study might enhance the research and development of unexplored three-phase UHTC composites which are applicable for "No. 7 energy problems in SDGs (Sustainable Development Goals)" in the future.

Acknowledgements

This work was financially supported by an advanced technological research project, "Research and Development Center for Advanced Composite Materials" of Doshisha University by MEXT (the Ministry of Education, Culture, Sports,

Science, and Technology, Japan)—supported Program for the Strategic Research Foundation at Private Universities, 2013-2017, project S1311036. The authors thank Ms Miwako Toda and Mr. Koji Ooka of the Doshisha University Research Centre for Interfacial Phenomena, for the FE-SEM and TEM observations of the samples.

Funding

This research was supported by the above-mentioned grant from MEXT.

Conflicts of Interest

The authors declare no conflicts of interest regarding the publication of this paper.

References

[1] Fahrenholtz, W.G. and Hilmas, G.E. (2017) Ultra-High Temperature Ceramics: Materials for Extreme Environments. *Scripta Materialia*, **129**, 94-99. https://doi.org/10.1016/j.scriptamat.2016.10.018

[2] Shaffer, P.T.B. (1991) Engineering Properties of Carbides. In: Schneider, S.J., Ed., *ASTM Engineered Materials Handbook*, *Vol.* 4 *Ceramics and Glasses*, ASM International, Almere, 804-811.

[3] Hampshire, S. (1991) Engineering Properties of Nitrides. In: Schneider, S.J., Ed., *ASTM Engineered Materials Handbook*, *Vol.* 4 *Ceramics and Glasses*, ASM International, Almere, 812-820.

[4] Cutler, R.A. (1991) Engineering Properties of Borides. In: Schneider, S.J., Ed., *ASTM Engineered Materials Handbook*, *Vol.* 4 *Ceramics and Glasses*, ASM International, Almere, 787-803.

[5] Fahrenholtz, W.G. and Hilmas, G.E. (2007) Refractory Diborides of Zirconium and Hafnium. *Journal of the American Ceramic Society*, **90**, 1347-1364. https://doi.org/10.1111/j.1551-2916.2007.01583.x

[6] Zhu, S., Fahrenholtz, W.G. and Hilmas, G.E. (2007) Influence of Silicon Carbide Particle Size on the Microstructure and Mechanical Properties of Zirconium Diboride-Silicon Carbide Ceramics. *Journal of the European Ceramic Society*, **27**, 2077-2083. https://doi.org/10.1016/j.jeurceramsoc.2006.07.003

[7] Hwang, S.S., Vasiliev, A.L. and Padture, N.P. (2007) Improved Processing and Oxidation-Resistance of ZrB_2 Ultra-High Temperature Ceramics Containing SiC Nanodispersoids. *Materials Science and Engineering*: *A*, **464**, 216-224. https://doi.org/10.1016/j.msea.2007.03.002

[8] Rezaie, A., Fahrenholtz, W.G. and Hilmas, G.E. (2007) Effect of Hot-Pressing Time and Temperature on the Microstructure and Mechanical Properties of ZrB_2—SiC. *Journal of Materials Science*, **42**, 2735-2744. https://doi.org/10.1007/s10853-006-1274-2

[9] Le, T.D., Hirota, K., Kato, M., Miyamoto, H., Yuasa, M. and Nishimura, T. (2020) Fabrication of Dense ZrB_2/B_4C Composites Using Pulsed Electric Current Pressure Sintering and Evaluation of Their High-Temperature Bending Strength. *Ceramics International*, **46**, 18478-18486. https://doi.org/10.1016/j.ceramint.2020.04.153

[10] Hirota, K., Shima, M., Chen, X., Goto, N., Kato, M. and Nishimura, T. (2015) Fabrication of Dense B_4C/CNF Composites Having Extraordinary High Strength and

Toughness at Elevated Temperatures. *Materials Science and Engineering*: *A*, **628**, 41-49. https://doi.org/10.1016/j.msea.2015.01.020

[11] Hirota, K. Nakayama, Y., Nakane, S., Kato, M. and Nishimura, T. (2008) The Study on Carbon Nanofiber (CNF)-Dispersed B_4C Composites. *International Journal of Applied Ceramic Technology*, **6**, 607-616. https://doi.org/10.1111/j.1744-7402.2008.02323.x

[12] Tsuchida, T. and Yamamoto, S. (2004) MA-SHS and SPS of ZrB_2–ZrC Composites. *Solid State Ionics*, **172**, 215-216. https://doi.org/10.1016/j.ssi.2004.05.020

[13] Tokita, M. (1993) Trends in Advanced SPS Spark Plasma Sintering Systems and Technology. *Journal of the Society of Powder Technology*, *Japan*, **30**, 790-804. https://doi.org/10.4164/sptj.30.11_790

[14] Neuman, E.W., Hilmas, G.E. and Fahrenholtz, W.G. (2016) Ultra-High Temperature Mechanical Properties of a Zirconium Diboride- Zirconium Carbide Ceramic. *Journal of the American Ceramic Society*, **99**, 597-603. https://doi.org/10.1111/jace.13990

[15] Tamamushi, F., Tomiyama, K., Kotani, M., Ando, T., Takahashi, H., Kubo, R., Nagakura, S. and Inoue, T. (1981) Dictionary for Physics and Chemistry, 3rd Edition, Iwanami Shoten, Tokyo, 1267.

[16] Niihara, K., Morena, R. and Hasselman, D.P.H. (1982) Evaluation of K_{IC} of Brittle Solids by the Indentation Method with Low Crack-to-Indent Ratios. *Journal of Materials Science Letters*, **1**, 13-16. https://doi.org/10.1007/BF00724706

[17] Huang, Z. and Wu, L. (2018) Phase Equilibria Diagrams of High Temperature Non-Oxide Ceramics. Springer, Singapore, 117. https://doi.org/10.1007/978-981-13-0463-7

[18] Shackelford, J.F. and Alexander, W. (2001) Materials Science and Engineering Handbook, 3rd Edition, CRC Press, New York.